Self-healing of Al_2O_3 containing Ti microparticles

Boatemaa, L.; van der Zwaag, S.; Sloof, W. G.

DOI
10.1016/j.ceramint.2018.03.119

Publication date
2018

Document Version
Final published version

Published in
Ceramics International

Ceramics International 44 (2018) 11116–11126

Contents lists available at ScienceDirect

Ceramics International

journal homepage: www.elsevier.com/locate/ceramint

Self-healing of Al_2O_3 containing Ti microparticles

L. Boatemaa[a,*], S. van der Zwaag[b,c], W.G. Sloof[a]

[a] Department of Materials Science and Engineering, Delft University of Technology, Mekelweg 2, 2628 CD Delft, The Netherlands
[b] Faculty of Aerospace Engineering, Delft University of Technology, Kluyverweg 1, 2629 HS Delft, The Netherlands
[c] School of Materials Science and Engineering, Tsinghua University, Beijing 100084, China

ARTICLE INFO

Keywords:
Self-healing
Alumina composite
Titanium
Isothermal oxidation
High temperatures

ABSTRACT

This work explores the possibility of using embedded micron-sized Ti particles to heal surface cracks in alumina and to unravel the evolution of the crack filling process in case of pure solid-state oxidation reactions. The oxidation kinetics of the Ti particles is studied and the results are applied in a simple model for crack-gap filling. An activation energy of 136 kJ/mol is determined for the oxidation of the Ti particles having an average particle size of 10 μm. The almost fully dense alumina composite containing 10 vol% Ti has an indentation fracture resistance of 4.5 ± 0.5 MPa $m^{1/2}$. Crack healing in air is studied at 700, 800 and 900 °C for 0.5, 1, and 4 h and the strength recovered is measured by 4-point bending. The optimum healing condition for full strength recovery is 800 °C for 1 h or 900 °C for 15 min. Crack filling is observed to proceed in three steps i.e., local bonding at the site of an intersected Ti particle, lateral spreading of the oxide and global filling of the crack. It is discovered that, although significant strength recovery can be attained by local bonding of the intersected particles, full crack filling is required to prevent crack initiation from the damaged region upon reloading. The experimental results observed are in good agreement with the predictions of a simple discrete crack filling/healing model.

1. Introduction

In recent years, material scientists have turned to the concept of *'damage management'* rather than *'damage prevention'* when re-designing engineering materials to make them more reliable for various applications [1]. This concept, also known as self-healing, is based on the notion that the formation of damage is not problematic as long as it is autonomously and timely healed or repaired in-situ as this would ensure the continued safe operation of the component or part.

In the original field-defining studies on self-healing materials, polymeric matrices were healed by incorporating capsules containing a liquid healing agent and a catalyst within the matrix [2]. As a crack propagates through the matrix, the microcapsules are ruptured and the catalyst particles are exposed, the healing agent flows into the crack and polymerizes once it gets into contact with one of the catalyst particles. The structural integrity across the crack plane is re-instated by the (solid) polymerized healing agent [3]. This type of healing is now categorized as extrinsic healing because healing is achieved by the addition of discrete foreign entities (i.e., the healing agent and the catalyst) to the (polymeric) matrix. It is also classified as autonomous healing as no additional trigger such as the supply of heat [4] is necessary to initiate the polymerization reaction leading to healing, i.e. the healing conditions in particular the temperature are the same as those during cracking (with the exception of the load responsible for the cracking having been removed).

In later years, ceramic oxides composites such as Al_2O_3, ZrO_2 and mullite filled with discrete solid healing particles prone to undergo oxidative expansive decomposition have also been studied as promising autonomous self-healing systems for high temperature applications [5–10]. Although the initial damage is generally introduced at room temperature the healing is realized by exposure to the intended use conditions, i.e. an oxygen-containing atmosphere heated to a suitably high temperature [4,11]. At such high temperatures, an oxidation reaction is initiated and the crack is filled with the reaction products. In case the oxide adheres well to the crack faces and the degree of filling is high enough, the load-bearing capacity of the composite is restored.

In an earlier study [12], 6 physical and chemical criteria were used to identify suitable healing particles to be used in the creation of high-temperature self-healing alumina composites. Experimentally the approach has been found to work well for alumina composites containing

* Corresponding author.
E-mail address: l.boatemaa@tudelft.nl (L. Boatemaa).

https://doi.org/10.1016/j.ceramint.2018.03.119
Received 29 January 2018; Received in revised form 12 March 2018; Accepted 13 March 2018
Available online 14 March 2018

either 15 or 20 vol% TiC [13] or SiC [8,10] particles, in agreement with the predictions of the selection model. Although that selection study did identify the alumina-Ti as a potentially attractive self-healing system such composite material have not been made and tested yet. Cracks in alumina containing Ti healing particles should under the same conditions (temperature and time) heal faster than composites containing TiC as the oxidation of Ti leads to a larger volume expansion for an equal amount of Ti atoms [12]. And while not so relevant for the self-healing behaviour, the inclusion of ductile metallic particles in a brittle ceramic matrix may be beneficial from a mechanical properties perspective [14]. In addition, dilute Al_2O_3-Ti composites retain their low coefficient of thermal expansion (CTE) and have a relatively high strength to weight ratio [15].

This work, therefore, investigates the high-temperature healing behaviour of an Al_2O_3 composite containing 10 vol% Ti particles with an average size of 10 μm. The activation energy and the temperature window available for self-healing are studied through thermal analysis of the oxidation kinetics of the Ti particles. Another very important and unique aspect of this work is the determination of the evolution of the crack filling and the semi-quantitative description of how the solid-state formation of TiO_2 leads to re-bonding of the cracked surfaces and restores the load-bearing capacity of the composite. For Al_2O_3 self-healing composites containing SiC, the healing agent formed (i.e., SiO_2) is amorphous during the early stages of the high-temperature oxidation process [16,17] and the amorphous character generates a viscous behaviour leading to liquid-like spreading of the reaction product into the crack. The ability of solid TiO_2 to '*spread*' into the crack gap and filling it as well as bond with the crack faces is of equal interest but has not been documented yet. Finally, the experimental observations on crack healing are compared to a simple model to predict the filling fraction as a function of time, temperature and original structure of the Al_2O_3–Ti composite.

2. Crack gap filling model

2.1. Background

Consider a ceramic composite with randomly distributed spherical healing particles; see Fig. 1. When fracture occurs, a planar crack of uniform width w is assumed to intersect the dispersed particles and at the appropriate temperature the intersected Ti particles oxidize into an oxide. The specific volume increase ϕ per particle due to oxidation is given by:

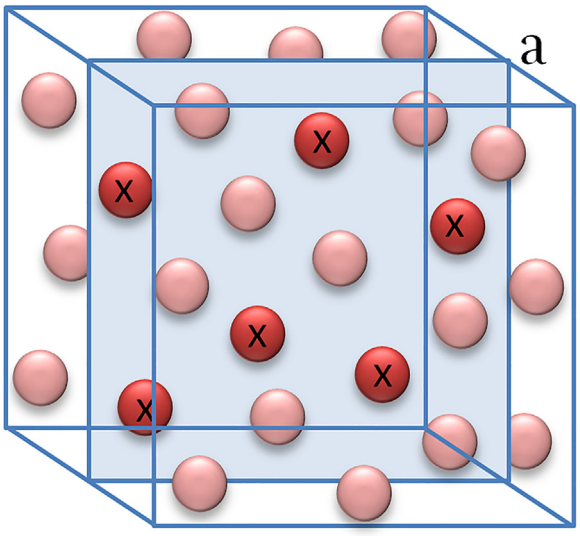

Fig. 1. A representative unit volume of a ceramic matrix composite containing randomly distributed spherical healing particles with plane 'a' intersecting the volume element.

$$\phi = \frac{V_{ox} - V_p}{V_p} \tag{1}$$

where V_{ox} and V_p are the molar volumes of the oxide (healing oxide) and the particle (healing particle) respectively.

Now consider a representative unit volume V_u of the self-healing composite containing evenly distributed spherical particles (each of diameter d) which is crossed by a plane a of area A_u as in Fig. 1 (the particles intersected by the plane are marked with a cross). If p is the probability that a planar crack crosses a healing particle, then:

$$p = d\frac{A_u}{V_u}, \quad \text{with } A_u = V_u^{2/3} \text{ implies } p = \frac{d}{V_u^{1/3}} \tag{2}$$

This implies that the number of healing particles n_p exposed to the crack is:

$$n_p = pN_p \text{ with } N_p = \frac{\varphi V_u}{V_p}, \text{ and } V_p = \frac{\pi d^3}{6} \tag{3}$$

N_p is the total number of spherical capsules present inside the unit volume element and φ is the volume fraction of healing particles added to V_u, then:

$$n_p = \frac{d}{V_u^{1/3}}\frac{6\varphi V_u}{\pi d^3} = \frac{6\varphi V_u^{2/3}}{\pi d^2} \tag{4}$$

Next, the volume of oxide filling the crack is:

$$V_f = \alpha_p \phi n_p V_p = \alpha\phi\varphi d V^{2/3} \tag{5}$$

where α_p is the fraction of the particle converted into the oxide. The volume of the gap with a width w to be filled is defined as:

$$V_g = wA_u = wV_u^{2/3} \tag{6}$$

Let ψ be the fraction of the crack gap filled, i.e.:

$$\psi = \frac{V_f}{V_g} \tag{7}$$

Eq. (7) can be rewritten in terms of Eqs. (4)–(6) as:

$$\psi = \frac{\alpha_p \phi \varphi d}{w} \tag{8}$$

A first order estimate of the early stages of crack filling can be made if all parameters in Eq. (8) are known. The volume expansion ϕ, the volume fraction healing particles φ and their size d are input parameters and are known up front, while the crack gap width w, on the other hand, can be chosen or measured once the damage is introduced into the material. Please note that in this simple model the filling fraction can be larger than 1 for small crack widths as the oxidation continues even when the crack is fully filled. The conversion of the healing particle into the healing oxide represented by α_p depends on (absolute) temperature and time:

$$\alpha_p = \alpha_p(T, t) \tag{9}$$

which is related to the oxidation of the healing particles.

2.2. Oxidation kinetics of the healing particles

The rate of a solid-state isothermal reaction can be expressed by the following general equation:

$$\frac{d\alpha}{dt} = Ae^{\left(-\frac{E_A}{RT}\right)} f(\alpha) \tag{10}$$

where α is the fraction converted at any time t. In case of an oxidation reaction it can be defined as: $\alpha = (m_t - m_0)/(m_\infty - m_0)$, in which m_0, m_t and m_∞ denote the mass at time t is *0*, t and ∞, $f(\alpha)$ is a differential form of the reaction model, E_A *is* the activation energy, A is the pre-exponential (frequency) factor of the Arrhenius relation, and T the absolute temperature [18]. Separating variables and integrating Eq. (10) gives the integral form of the isothermal rate law:

$$g(\alpha) = kt \tag{11}$$

$$\text{where } g(\alpha) = \int_0^{\alpha} \frac{d(\alpha)}{f(\alpha)} \tag{12}$$

$$\text{and } k = Ae^{\left(-\frac{E_A}{RT}\right)} \tag{13}$$

$g(\alpha)$ is the integral reaction model and k is the rate constant. There are several reaction models which are classified based on the shape of their isothermal curves [19]. When the appropriate model for the reaction is identified, the conventional isothermal model-fitting method can be employed to determine the activation energy E_A and frequency factor A. This method involves two fits: the first determines the rate constant k of the reaction at each temperature according to Eq. (11) and the second determines the Arrhenius constant A and the E_A from Eq. (13). Then, an expression for α can be written.

2.3. Reaction model

To determine the appropriate model to analyze the experimental data the so-called 'master curve plotting' method is employed. This method is based on the concept of generalized time θ [18], which is defined for an isothermal reaction as:

$$\theta = \int_0^t e^{\left(\frac{-E_A}{RT}\right)} dt \text{ or } \frac{d\theta}{dt} = e^{\left(\frac{-E_A}{RT}\right)} \tag{14}$$

θ denotes the reaction time taken to attain a particular fraction converted at infinite temperature. Now, Eqs. (10) and (14) can be rewritten in terms of generalized time respectively as:

$$\frac{d\alpha}{d\theta} = Af(\alpha) \tag{15}$$

$$g(\alpha) = A\theta \tag{16}$$

As a reference point for the master-curve plotting analysis generally, the level $\alpha = 0.5$ is chosen and using Eq. (15) it can be derived that:

$$\frac{d\alpha/d\theta}{(d\alpha/d\theta)_{\alpha=0.5}} = \frac{f(\alpha)}{f(0.5)} \tag{17}$$

From the experimentally determined conversion rate, with respect to the generalized time, as a function of fraction converted, $f(\alpha)/f(0.5)$ vs α can be obtained, since:

$$\frac{d\alpha}{d\theta} = \frac{d\alpha}{dt}\exp\left(\frac{E_A}{RT}\right) \text{ or } \frac{d\alpha}{d\theta} = \beta\frac{d\alpha}{dT}\exp\left(\frac{E_A}{RT}\right) \tag{18}$$

Therefore, Eq. (17) becomes:

$$\frac{d\alpha/d\theta}{(d\alpha/d\theta)_{\alpha=0.5}} = \frac{d\alpha/dt}{(d\alpha/dt)_{0.5}}\frac{\exp(E_A/RT)}{\exp(E_A/RT)} \tag{19}$$

For the experimental kinetic data under isothermal conditions, the exponential terms in Eq. (19) cancel out since $T_t = T_{0.5}$. By comparing the experimental result with theoretical reaction models [18], the reaction model that best fits the measured data can be determined.

2.4. Activation energy and Arrhenius constant

The activation energy is evaluated from the slope of the plot of $\ln k$ vs $1/T$ using the Arrhenius relation defined by Eq. (13) and the intercept gives the Arrhenius constant A. First, the rate constants are evaluated at each temperature from the linear relation between the integral form of the identified reaction model and time, given by Eq. (11).

3. Experimental procedure

The starting materials were commercially available alumina powder (AKP-50, Sumitomo Chemical Co., Ltd, Tokyo, Japan) with an average particle size of 0.2 μm and Ti powder (PN: TI-M-02M-MP.05UMS, American elements, USA) with an average particle size of 10 μm. The purity of the alumina and Ti powder is 99.99% and 99.45%, respectively. The size distribution of the powders was measured by laser diffraction using a Microtrac 3500 (Microtrac Inc., USA). The particle size of the Ti powder was found to range from 4 to 15 μm with an average size of 10 μm. The phase purity and composition of the Ti powder was analyzed by X-ray diffraction (XRD) using a Bruker D8 Advance diffractometer (Bruker, Germany) with a graphite monochromator and Co Kα radiation. The diffractograms were processed with the accompanying software Diffrac.EVA 4.1 from Bruker. The shape of the Ti particles and the microstructure of the composite were observed with scanning electron microscopy (SEM) using a JSM 6500FD (JEOL, Japan). After healing the extent of filling was observed with SEM and the reaction products were analyzed by X-ray microanalysis (XMA) using the energy dispersive spectrometer (EDS) attached to the scanning electron microscope. This EDS is an Ultra Dry detector (30 mm^2) operated with Noran System Seven software package (ThermoFisher, USA) for data acquisition and analysis.

The oxidation kinetics of the Ti particles was studied isothermally over the temperature range from 600 to 850 °C (with increments of 50 °C) by thermogravimetric analysis (TGA) using the Setsys Evolution 16 simultaneous thermal analyzer (Setaram, France). 20 ± 1 mg of the Ti powder was put into an Al_2O_3 crucible (100 μL) and the furnace was heated up from room temperature at 5 °C/min under pure N_2 (with H_2O < 10 ppm) supplied at 50 sccm, when the desired temperature was reached the flow of N_2 was reduced by 20 vol% and replaced by O_2 thereby generating synthetic air in the furnace. The mass change curves were corrected using blank measurements under similar conditions.

A composite of Al_2O_3 containing 10 vol% of Ti was prepared by first mixing the powders. To avoid agglomeration of the Ti particles an alkali-free organic polyelectrolyte Dolapix CE64 (Zschimmer & Schwarz, Germany) was added as a surfactant [20]. This aided in the homogenous distribution of the healing particles; see Fig. 2a. In the absence of the polyelectrolyte, the Ti particles remained stuck to each other as shown in Fig. 2b.

The powders were mixed using distilled water as the liquid media. The mass fractions as used for mixing were 50% of powders, 45% of distilled water and 5% of the surfactant. Mixing was done using zirconia balls (of diameters 5 and 10 mm) in a planetary ball mill PM 100 (Retsch, Germany), the powder to ball mass ratio was 2:1. The suspension was mixed for 6 h at 150 rpm with an on-and-off period of 20:10 min. The slurry was left to dry overnight at 90 °C for 16 h. Then the cake was grounded and passed through 200, 120 and 50 μm sieves before sintering in a spark plasma sintering (SPS) furnace. The evenly mixed powder was packed into a 40 mm graphite mold and heated at 20 °C/min up to 1300 °C and held for 10 min in argon under 50 MPa for SPS in an HPD 25 SD furnace (FCT Systeme, Germany). After sintering the system was cooled naturally after lifting up the pistons. The density of the composite was measured by the Archimedes method using an analytical balance (Mettler Toledo AG-204, Switzerland) according to ASTM B 311-93.

To study the strength recovery, the sintered composite discs were machined to 3.0 × 4.0 × 26.0 mm rectangular bars with beveled edges. The surfaces of the bars were polished to a mirror finish with 1 μm diamond suspension. Cracks were introduced at the centre of the bar by means of Vickers' indentation using a Zwick/Z2.5 hardness tester (Zwick, Germany) operated in force controlled mode of 5 N/s with a maximum load of 20 N held for 20 s at load. The cracks formed were parallel and perpendicular to the long axis of the sample.

The indentation fracture resistance of the composite was measured by making several indents at 10, 20, 50 and 100 N. The indent size $2a$ and the crack length $2c$ defined respectively as the average of the diagonals of the imprint made by the indent and the average of the horizontal and vertical cracks formed in addition to the indent size was measured at the various loads. The length of cracks generated was then used in calculating the composite's fracture toughness. Annealing of the

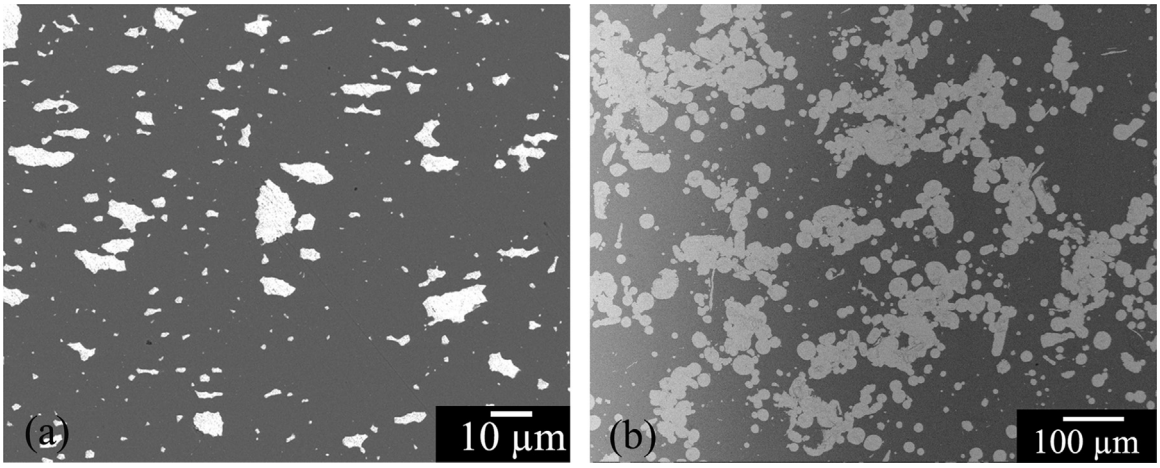

Fig. 2. Microstructure of the Al_2O_3 Ti composite showing the distribution of Ti (white phase) in alumina produced with (a) and without (b) adding the surfactant Dolapix.

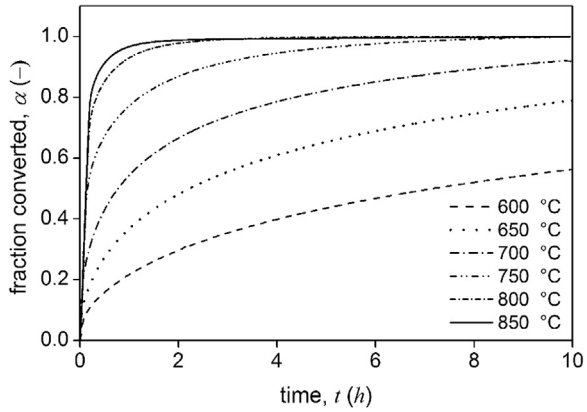

Fig. 3. Fraction of Ti powder converted to TiO_2 α, in dry synthetic air as a function of time t, for different annealing temperatures.

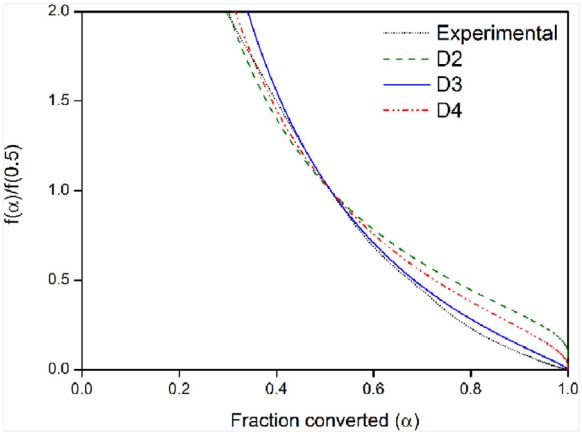

Fig. 4. Master plot of theoretical models and experimental data of Ti oxidation.

cracked samples to induce partial or full filling of the indentation cracks was carried out in a Carbolite TZF 17/600 furnace (Carbolite Gero, UK) at 700, 800 and 900 °C for 0.5, 1, and 4 h filled with natural air. The strength recovered was measured by 4-point bending tests which were performed at room temperature on a self-aligning stage [13]. This stage has a 20/10 mm span with hardened steel rollers 2 mm diameter. The stage was mounted to an Instron 5500R (Instron Corporation, USA) material testing frame with a 10 kN load cell. The cross-head was displaced at a velocity of 0.5 mm/min and the bar specimen was placed so that its centre coincides with the middle of the spans.

Table 1
Rate constant k values found from linear fitting of Eq. (11) at different temperatures.

T (°C)	k (s^{-1})
600	0.0058
650	0.0162
700	0.0313
750	0.0722
800	0.2212
850	0.2968

4. Results

4.1. Kinetics of Ti particle oxidation

The oxidation kinetics of the Ti particles between 600 and 850 °C was determined from the mass gain measured (cf. Section 2.2) and the results are presented in Fig. 3.

The oxidation kinetics of the collection of Ti particles between 600 and 900 °C is diffusion controlled as mentioned in [21], and the rate is mainly governed by dissolution of oxygen in the metal. The oxidation rate decreases with time due to the increasing thickness of the oxide shell which acts as a strong diffusion barrier, see Fig. 3. At the studied temperatures, only rutile (TiO_2) formed according to the XRD data. Other phases such as; Ti_2O, TiO and Ti_3O_5 only form at higher temperatures and low oxygen partial pressure levels [21]. From Fig. 3 and [19], it is clear that the oxidation of Ti follows a deceleratory model and the master plotting method, see Fig. 4, confirms that the reaction best conforms to a D3 diffusion model.

The integral form of the D3 diffusion model is given by:

$$g(\alpha) = (1 - (1 - \alpha)^{1/3}) \quad (20)$$

Although Ginstling-Brounshtein [22] have shown that this equation is invalid for higher conversion fractions or longer reaction times, it can be used as a first order approximation for lower conversion fractions yielding with Eq. (11):

$$\alpha = 1 - (1 - \sqrt{kt})^3 \quad (21)$$

A linear fitting of the fraction converted at each temperature according to Eq. (11), using the D3 model yielded the various k values presented in Table 1.

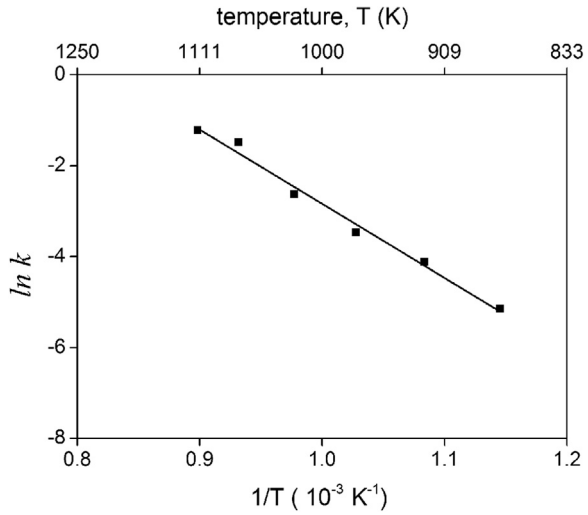

Fig. 5. Arrhenius plot of ln k vs 1/T to determine the activation energy for oxidation of 10 μm sized Ti powder.

The activation energy is determined from the slope of the plot in Fig. 5. It is evaluated to be 137 ± 9 kJ/mol. The lower value in comparison to that of bulk Ti (213 kJ/mol [23]) may be due to the much larger density of surface defects of the particles. This difference in activation energy cannot be explained by the variation of surface bonding states due to surface curvature constraints, since the particles are of micron rather than nano size [24].

4.2. Mechanical properties of the Al_2O_3-Ti composite

The sintered samples were very dense with densities between 97.7% and 99.2% of the calculated theoretical density. A cross-sectional view of the indented surface shows that the 20 N load generated cracks had a half-penny shaped geometry of about 20 μm in radius, see Fig. 6. This is a common morphology for Vickers indentation induced cracks [25] and hence the indentation fracture resistance of the composite was evaluated according to [26].

For composite materials containing well dispersed particles, cracks propagate through either the matrix, along the interface or through the particles, depending on which path is energetically most favourable. The lower modulus of Ti (110 GPa [27]) with respect to Al_2O_3 (380–410 GPa [28]) leads to the crack being attracted to the Ti particles [29], rendering it the preferred crack path as shown in Fig. 7.

The indentation fracture resistance of the composite is evaluated by

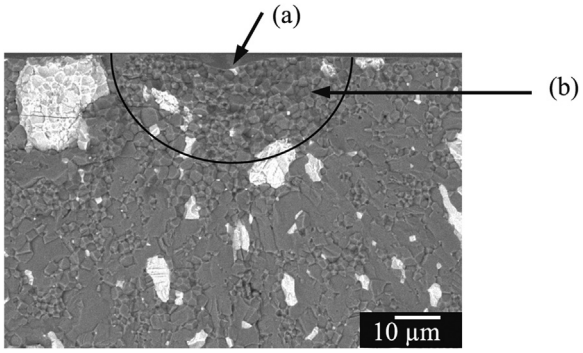

Fig. 6. Cross section of indented surface (a) Marks the imprint of the indent and (b) The half-penny crack.

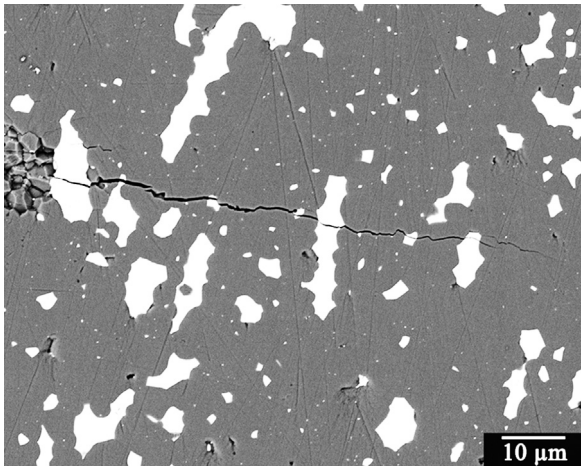

Fig. 7. Crack particle interaction showing cracks running through the softer Ti phase. Grey area is alumina and the white patches are Ti particles.

making several cracks by Vickers indentation at different loads (i.e., at 10, 20, 50 and 100 N). From the indent size *2a* and crack length *2c*, the indentation fracture resistance of Al_2O_3 containing 10 vol% of Ti particles of average size 10 μm is evaluated to be 4.5 ± 0.5 MPa $m^{1/2}$. This compares well with the fracture toughness as measured for Al_2O_3 composites containing either 20 vol% TiC [13] or 20 vol% Ti_2AlC [30], 4.3 ± 0.1 MPa $m^{1/2}$ and 4.9 ± 0.5 MPa $m^{1/2}$ respectively.

4.3. Evolution of crack filling

To proof that Ti particles embedded in Al_2O_3 can heal surface cracks, a crack of length *2c* about 100 μm was made and healed at 800 for 4 h. After healing, the cracks emerging from the corners of the Vickers indent were observed using SEM to be fully covered with a light coloured material confirmed by X-ray microanalysis to be TiO_2; see Fig. 8a. After removal of the surface oxides by gentle polishing, the whole length of the crack was found to be filled with TiO_2 even though Ti particles were not identified everywhere along the length of the crack; see Fig. 8b.

The evolution of the crack-gap filling process was investigated by annealing a sample with several indents at a fixed temperature of 700 °C for different times and observing the extent of filling after every annealing exposure. The healing temperature was selected at 700 °C as the kinetics at this temperature is relatively slow. The microscopic images for two different areas taken after 1, 2, 4 and 6 h of exposure are presented in Figs. 9 and 10. From the observations it is concluded that the crack filling proceeds in 3 successive steps:

In the first step, 'hairy' oxides grow on crack-intersected particles. These hairy oxides on opposite sides of the crack grow into each other (i.e., intertwine) leading to the local bonding of the healing particle, see Fig. 9b and c. This step is hereafter referred to as the local bonding step. In the second step, the oxides from the intersected particles grow laterally into the crack, see Fig. 10b, and c, but can still be clearly connected to the particle from which they stem. This second step is called the lateral spreading step. Finally, there are areas along the crack with no intersected particles, yet oxides are seen filling and sprouting out of the cracks; see Figs. 9 and 10d and e. This results from oxidation of particles that are exposed in the depth of the crack. This step is called the global filling step. Local bonding and lateral spreading are thought to occur consecutively; however, global filling occurs simultaneously

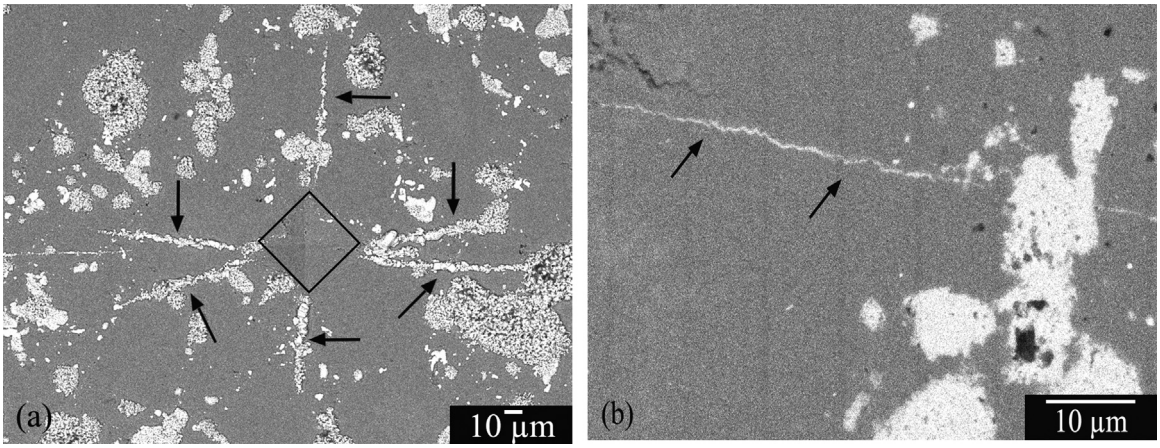

Fig. 8. Grey area is Al_2O_3 and white area is TiO_2. (a) All cracks are fully filled with TiO_2 indicated by arrows. (b) Surface oxide removed to show full filling of a crack of about 50 µm in length. Arrows indicate a fully filled crack without Ti particles on the crack path.

with steps 1 and 2, provided enough oxygen reaches the intersected Ti particles further below the surface.

The *spreading or flowing* mechanism was studied in more detail by SEM recordings of cross-sections of a sample fractured after healing and by the stepwise planar removal of material from a partially healed sample.

For the cross-sectional analysis, the sample was healed at 800 °C for 30 min and fractured. The crack was not fully filled and so acted as a crack initiator causing the sample to break into 2 equal halves along the path of the indent. A cross section of the fractured surface showing the semi-circular crack front and the imprint of the indent is shown in Fig. 11.

A zoom-in of two areas on the crack plane of Fig. 11, is presented in Fig. 12. Three different phases associated with the matrix (darker grey), healing particle (white) and healing oxide (lighter grey), respectively, can be distinguished in both micrographs.

Next, X-ray mapping of Fig. 12b is performed to affirm the presence of TiO_2 (healing oxide) on the crack surface and the results are presented below in Fig. 13. In Fig. 13b, oxygen is identified over the whole surface except for the Ti particles (in white). Ti is identified and mapped in blue over a larger area in Fig. 13c, (in the bigger ellipse) an area larger than where only Ti was detected in Fig. 13b. The overlap of Ti and O within the larger ellipse indicates the presence of TiO_2 on the crack surface. This is a clear evidence of crack filling by a particle in the plane of the crack. With time TiO_2 continues to form from such particles in the crack plane, the oxides spreads over the crack surface and fill the crack outwards contributing to global filling as depicted in Figs. 9 and 10(d and e).

Next, looking at the stepwise planar removal of material (parallel to the original sample surface) of an untested but partially healed sample which was annealed at 800 °C for 1 h to observe crack filling as a function of the depth of the crack. The results from two different cracks are presented in Figs. 14 and 15. A crack about 40 µm long that is fully filled with lots of surface oxides is presented in Fig. 14a. The surface oxides are removed in Fig. 14b to clearly show the fully filled crack intersection with the original sample surface. Ti particles, which directly contribute to crack filling (by local bonding and lateral spreading), are observed along the crack path at point M, N and O. However, at point P no Ti particle is identified, although the crack in this area is fully filled.

About 3 µm of surface material was removed by gentle polishing and the new surface observations are given in Fig. 14c. At this depth, part of the particle at point M still remains and the crack is filled in this area In contrast, the particles at points N and O are no longer present, yet, the crack at these areas is still fully filled. A new particle is now intersected by the crack at point P. Evidence presented in Fig. 12 suggests that global filling takes place 3 µm from the surface at point P, the oxide formed from this particle spread into the crack outwards to the surface as in Fig. 14b. Particles at point N and O may have also spread downwards into the crack and/or there may still be a particle buried deep in the crack which fills the crack upward.

Similarly, Fig. 15a shows a partially filled crack with surface oxides. After removal of the surface oxides in Fig. 15b, the area in the ellipse is not filled, although, oxides can be seen in the crack. After removal of about 3 µm thick material in Fig. 15c, the crack in the ellipse is filled with oxides from a particle exposed to the crack at this depth. This clearly illustrates global filling by a particle buried in the depth of the crack, which given enough time would have continued to fill the whole crack.

Figs. 9 and 10 have clearly illustrated the local bonding and lateral spreading stages of crack filling, while Figs. 12–15 prove the concept of global filling as particles identified along the crack path in the depth of the material significantly contribute to crack filling closer to the surface.

4.4. Strength-recovery

The pre-cracked samples were healed at 700, 800 and 900 °C for 0.25, 0.50, 1, 2 and 4 h, and the results of the post-healing fracture strength measurements are presented in Fig. 16. The original and the non-healed strength values are also included; each value plotted is the average of 8 samples tested per condition. The strength of the intact specimen was 335 ± 23 MPa and after indentation at 20 N a crack of length *c* of 35 µm was generated which decreased the initial strength by 32% to 228 ± 22 MPa. In the reference Al_2O_3-TiC composite [13] a bending strength decrease of about 50% has been reported for the same indentation damage conditions, confirming that the current Al_2O_3-Ti composite is as expected relatively ductile.

As shown in Fig. 16, the flexural strength was fully recovered after healing at 700 °C for 4 h, 800 °C for 1 h and at 900 °C for 30 min with

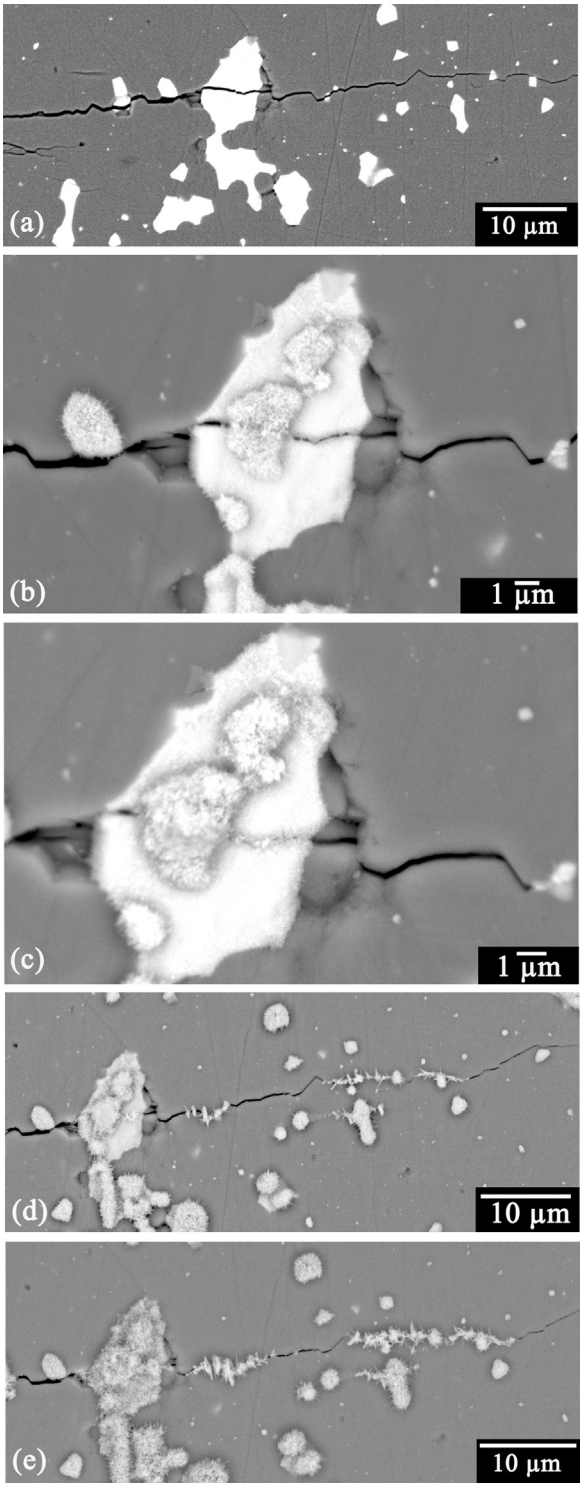

Fig. 9. Evolution of crack-gap filling of the Al_2O_3 containing 10 vol% of Ti by oxidation in air at 700 °C for different times. (a) Starting material, (b) Annealed after 1 h, (c) 2 h, (c) 4 h, and (e) 6 h.

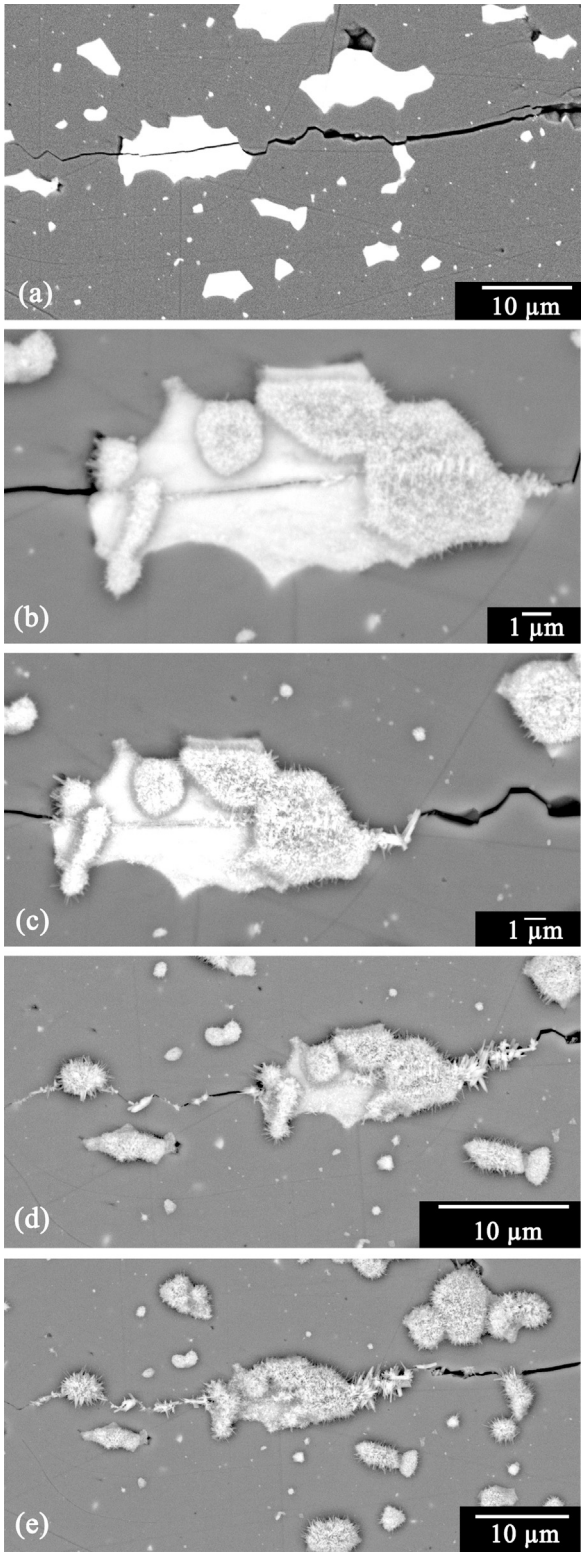

Fig. 10. Evolution of crack-gap filling of another area of the same sample as in Fig. 9. (a) Starting material, (b) Annealed after 1 h, (c) 2 h, (c) 4 h, and (e) 6 h.

average flexural strengths of 331, 350 and 360 MPa, respectively. The average bending strength values after extensive healing were found to be slightly higher than that of the original samples. This may have resulted from the filling of surrounding pores left behind after sintering. The period for the first set of healing experiments was reduced by half to find an optimum healing condition (lowest temperature and shortest time) at which full strength can be recovered. At 800 and 900 °C for 30 and 15 min, respectively, full strength was recovered at 329 and 347 MPa, respectively. However, at 700 °C for 2 h only 88% of the initial strength was recovered. The optimum healing condition for the studied composite is 800 °C for 1 h or 900 °C for 15 min.

Further analysis of the failure behaviour of samples after healing revealed that all samples kept at 800 °C for 1 h and at 900 °C for 15 and 30 min broke at positions not connected with those of the (healed)

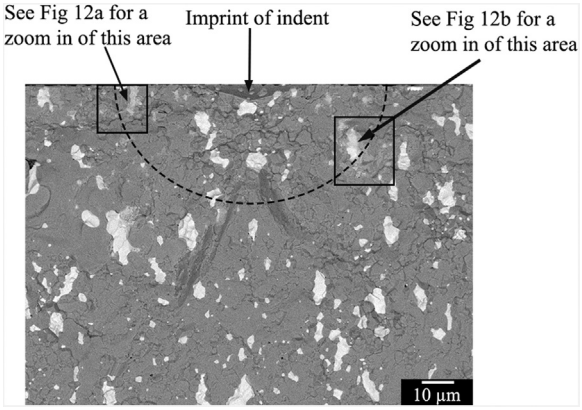

Fig. 11. Side view of a partially healed indentation induced crack after sample fracturing (see text).

indentation induced cracks. For those three conditions, the cracks observed were fully filled. For conditions at which the cracks were recorded to be been only partially filled (such as after healing at 800 °C for 30 min), it was observed that the crack plane was not fully covered with the healing oxide, see Fig. 12, however, local bonding and lateral spreading had occurred. The (room temperature) failure load was higher than after the indentation, but sample failure still took place at the sample centre (where the indent was made). Similarly, after healing at 700 °C for 2 h, cracks were partially filled with oxides from local bonding and lateral spreading with most of the samples failing along the centre. At this condition, Figs. 9c and 10c clearly depicts that there was no global filling. Finally, although cracks were not fully filled after 4 h at 700 °C, substantial global filling had taken place (see, Figs. 9d and 10d) leading to only 20% of the samples breaking along the centre. It can therefore be concluded that local bonding, which leads to bridging of the crack, significantly increases the residual strength, however, global filling is vital in obtaining a strong healed zone.

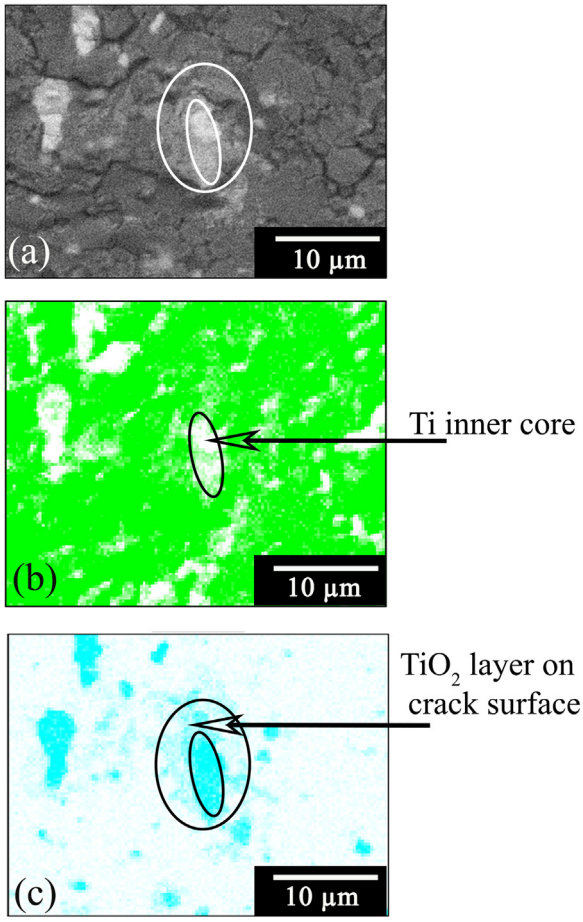

Fig. 13. (a) SEM image of a crack plane after annealing at 800 °C for 30 min in air, (b) O kα X-ray map and (c) Ti kα X-ray map of the same area.

4.5. Application of the crack-gap filling model

An estimate of the filling fraction ψ (i.e. the ratio of volume of oxide formed during healing with respect to the initial crack volume, cf. Eq. (8), can be obtained from the oxidation kinetics of the healing particles, see Eq. (21). However, as the surface area created when a particle is intersected by the crack is relatively small, more time is required for an embedded healing particle to fully transform than for a set of free particles as measured by thermogravimetric analysis; cf. Section 4.1. Therefore, the conversion of the healing particle into the healing oxide in Eq. (21) is modified to reflect the increased time required for the transformation of an embedded healing particle Eq. (9). Thus:

$$\alpha_p = \alpha(T, t{\cdot}f_A) \tag{22}$$

The area correction factor f_A is determined by comparing the area of the intersected particle, which is exposed to the crack gap, to the surface area of the free spherical particle as:

$$f_A = \frac{2\pi < r >^2}{4\pi r^2} \tag{23}$$

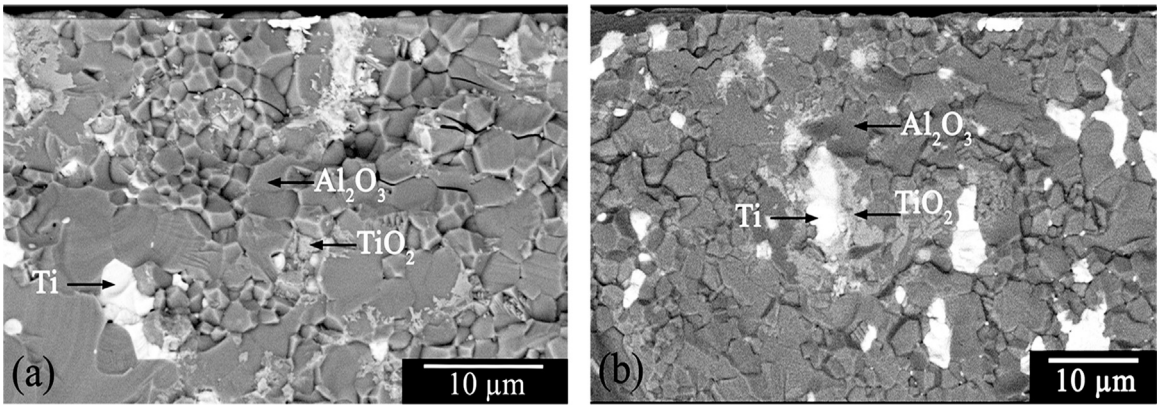

Fig. 12. SEM images of two different areas of the crack plane of a sample oxidized at 800 °C for 30 min showing the matrix, healing particle and the healing oxide that has spread onto the crack plane.

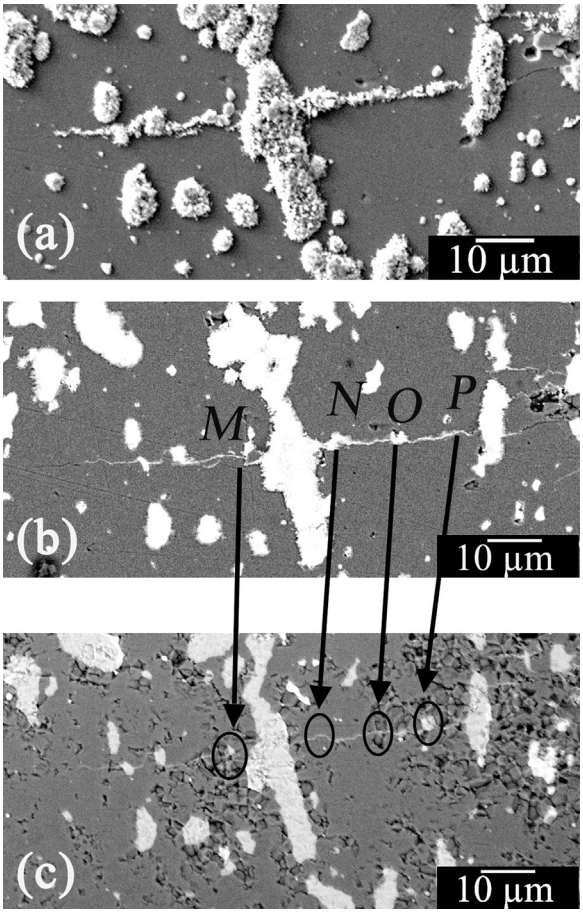

Fig. 14. SEM images after annealing at 800 °C for 1 h in air. (a) Fully filled crack with surface oxides. (b) Crack filling after removal of surface oxides. (c) After removal of about 3 µm thick material, particles at point M diminish, while that at N and O disappear, new particle which contributes to healing is identified at point P.

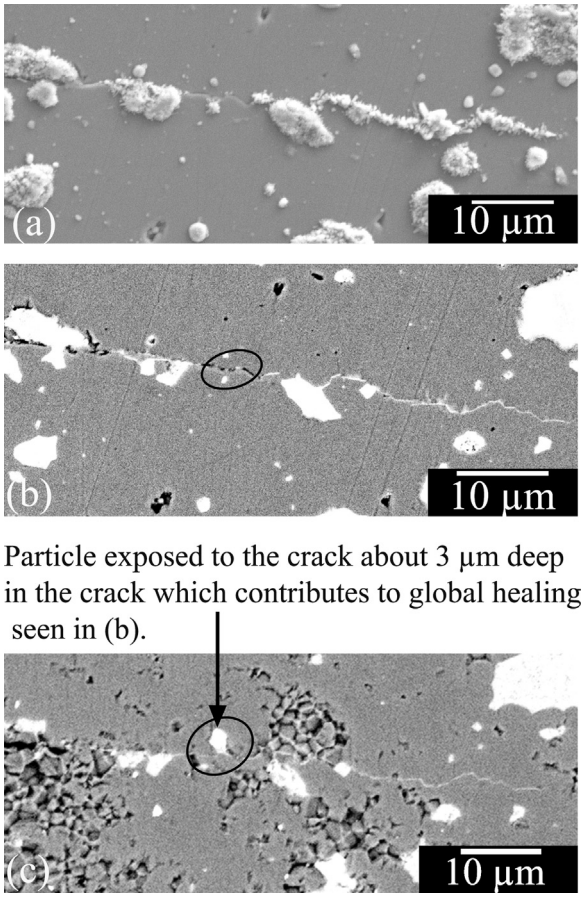

Fig. 15. SEM images annealing at 800 °C for 1 h in air. (a) Filled crack with surface oxides. (b) Crack not fully filled after removal of surface oxides. (c) Particle exposed to the crack 3 µm in the depth of the crack that oxidizes and spreads into the crack contributing to global filling.

where $<r>$ is the average radius of the surface of a randomly intersected spherical healing particle with radius r. It can be shown that:

$$<r> = \frac{\pi}{4} r \tag{24}$$

hence $f_A = \pi^2/32$ and the Eq. (8) for the early stage filling fraction becomes:

$$\theta = \frac{1 - (1 - \sqrt{kt \cdot f_A})^3}{w} \phi \varphi d \tag{25}$$

where all terms have the usual defined meanings, ϕ is 0.8 (i.e. conversion from Ti to TiO_2), φ is 0.1, d is 10 µm and w (measured during SEM observation) is 0.5 µm. The filling fraction computed from the model according to Eq. (25) at different temperatures is in good agreement with the experimental results; see Fig. 17.

For example, experimentally it has been determined that samples annealed at 900 °C for 15 min were fully healed while the model predicts full healing at about 20 min. Similarly, for samples annealed at 800 °C partial healing was observed after 30 min, while full healing was observed after 60 min. The model predicts that, 70 min is required for full strength recovery at this temperature. Finally, at 700 °C, all samples annealed for 120 min broke along the original crack path in accordance with a filling fraction of about 55% predicted by the model.

Next, the model is extended to predict the time when local bonding occurs at the studied temperatures. The intersected spherical particles will form cylindrical healing oxide bridges during local bonding across the width of the crack (w). The filling fraction required for this can be evaluated from:

$$\psi_{local} = n_p \frac{V_{bridge}}{V_g} \tag{26}$$

where n_p and V_g have been previously defined (cf. Eqs. (4) and (6), respectively) and V_{bridge} is the volume of the cylindrical oxide bridge formed between intersected particles.

$$V_{bridge} = \pi < r >^2 w \tag{27}$$

in which the average radius of the surface of a randomly intersected spherical healing particle is defined in Eq. (24). Now, the local bridging by the healing particles according to Eq. (26) becomes:

$$\psi_{local} = \frac{3\pi^2}{32} \varphi \tag{28}$$

and thus only depends on the volume fraction healing particles φ.

This minimal filling fraction required to establish the local bonding stage is evaluated to be 0.0925. This level is indicated in the insert in Fig. 17, where it is seen that at the studied temperatures local bonding can be established in a relatively short time (i.e. under 1 min at 800 and 900 °C and in about 4 min at 700 °C).

The influence of the crack opening distance on the filling fraction is analyzed using the optimum healing conditions from the experiments (i.e. 700 °C for 4 h, 800 °C for 1 h and 900 °C for 0.25 h). According to Eq. (8), the filling fraction is inversely proportional with the width of the crack and this relation is depicted in Fig. 18. It is observed that, at any temperature, doubling the crack width decreases the filling fraction

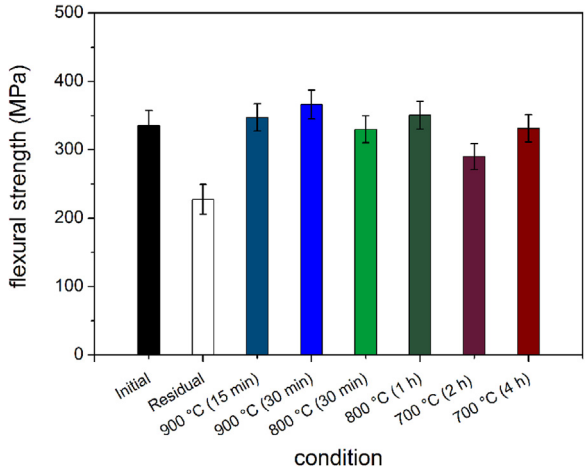

Fig. 16. Room temperature flexural strength values of the Al_2O_3-Ti composites before, after indentation damage and after healing at the indicated temperature-time combinations.

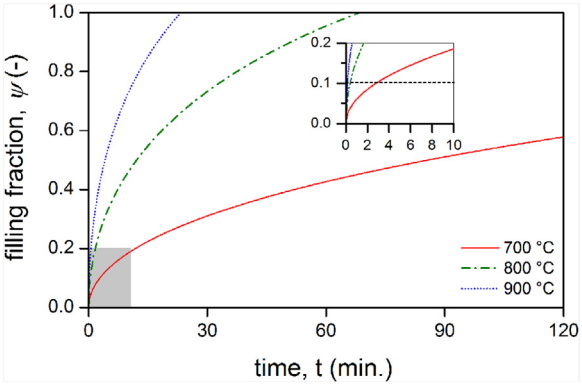

Fig. 17. Predicted filling fraction as function of time at different temperatures for an initial crack width of 0.5 μm and conditions as specified in the text. The line at 1.0 indicates full filling of the crack gap.

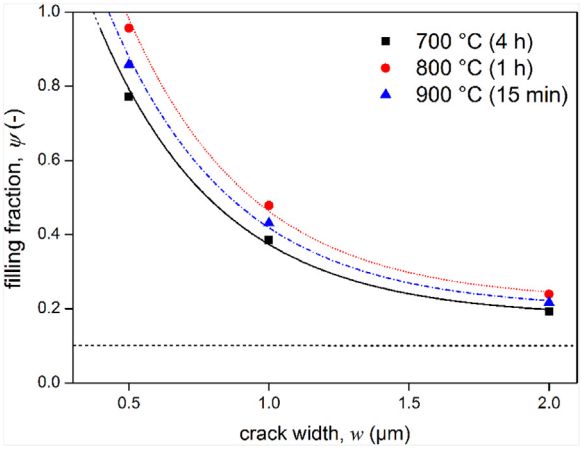

Fig. 18. Calculated fraction of the crack filled ψ as a function of crack width for different temperatures and specified times. The dashed line at 0.1 indicates the minimum filling required for the whole crack to be bridged in the local bonding stage and the line at 1.0 indicates full filling of the crack gap.

by about 50%, hence the width of the crack is identified as a sensitive parameter in strength recovery. It is also observed that the specified healing conditions local bonding is always established even at crack openings of up to 2 μm although the cracks will not be fully filled and will fail along the damaged region.

5. Conclusions

This work affirms the capability of embedded Ti particles to heal and close up surface cracks in Al_2O_3 by oxidation at high temperatures. In a dense Al_2O_3 based composite containing 10 vol% of Ti, room temperature Vickers indentation induced cracks with a radius of 20 μm and a width of less than 1 μm can be fully filled by annealing 800 °C for 1 h or 900 °C for 15 min. The full filling is accompanied by a full recovery of the bending strength at room temperature. The activation energy for oxidation and the indentation fracture toughness were evaluated to be 136 kJ/mol and 4.5 ± 0.5 MPa $m^{1/2}$, respectively. Crack filling proceeds in three steps: local bonding and lateral spreading and finally global filling which takes place provided oxygen reaches Ti particles buried in the crack plane. The bridging of cracks by local bonding leads to significant strength recovery but full crack filling through global filling is essential in obtaining a strong healed zone. The results from the kinetic crack-gap filling model are in good agreement with the experimental results.

Acknowledgements

This research was sponsored by the People Program (Marie Curie ITN) of the European Union's Seventh Framework Program, FP7, Grant no. 290308 (SHeMat). The authors are indebted to Dr. A.C. Riemslag for his assistance with mechanical testing.

References

[1] S. van der Zwaag, An introduction to material design principles: damage prevention versus damage management, in: S. van der Zwaag (Ed.), Self Healing Materials: An Alternative Approach to 20 Centuries of Materials Science, Springer, Netherlands, Dordrecht, 2007, pp. 1–18.
[2] E.N. Brown, N.R. Sottos, S.R. White, Fracture testing of a self-healing polymer composite, Exp. Mech. 42 (2002) 372–379.
[3] E.N. Brown, S.R. White, N.R. Sottos, Microcapsule induced toughening in a self-healing polymer composite, J. Mater. Sci. 39 (2004) 1703–1710.
[4] M.D. Hager, P. Greil, C. Leyens, S. van der Zwaag, U.S. Schubert, Self-healing materials, Adv. Mater. 22 (2010) 5424–5430.
[5] K. Houjou, K. Ando, K. Takahashi, Crack-healing behaviour of ZrO_2/SiC composite ceramics, Int. J. Struct. Integr. 1 (2010) 73–84.
[6] M. Ono, W. Nakao, K. Takahashi, M. Nakatani, K. Ando, A new methodology to guarantee the structural integrity of Al_2O_3/SiC composite using crack healing and a proof test, Fatigue Fract. Eng. Mater. Struct. 30 (2007) 599–607.
[7] K. Takahashi, K. Uchiide, Y. Kimura, W. Nakao, K. Ando, M. Yokouchi, Threshold stress for crack healing of mullite reinforced by SiC whiskers and SiC particles and resultant fatigue strength at the healing temperature, J. Am. Ceram. Soc. 90 (2007) 2159–2164.
[8] K. Takahashi, M. Yokouchi, S.-K. Lee, K. Ando, Crack-healing behavior of Al_2O_3 toughened by SiC whiskers, J. Am. Ceram. Soc. 86 (2003) 2143–2147.
[9] K. Ando, K. Furusawa, M.C. Chu, T. Hanagata, K. Tuji, S. Sato, Crack-healing behavior under stress of mullite/silicon carbide ceramics and the resultant fatigue strength, J. Am. Ceram. Soc. 84 (2001) 2073–2078.
[10] K. Ando, B.S. Kim, M.C. Chu, S. Saito, K. Takahashi, Crack-healing and mechanical behaviour of Al_2O_3/SiC composites at elevated temperature, Fatigue Fract. Eng. Mater. Struct. 27 (2004) 533–541.
[11] S.K. Ghosh, Self-healing Materials: Fundamentals, Design Strategies, and Applications, Self-Healing Materials, Wiley-VCH Verlag GmbH & Co. KGaA, Weinheim, 2009, pp. 1–28 ISBN: 978-3-527-31829-2.
[12] L. Boatemaa, C. Kwakernaak, S. van der Zwaag, W.G. Sloof, Selection of healing agents for autonomous healing of alumina at high temperatures, J. Eur. Ceram. Soc. 36 (2016) 4141–4145.
[13] S. Yoshioka, L. Boatemaa, S. van der Zwaag, W. Nakao, W.G. Sloof, On the use of TiC as high-temperature healing particles in alumina based composites, J. Eur. Ceram. Soc. 36 (2016) 4155–4162.

[14] J.R. Heffelfinger, R.R. Kieschke, C.B. Carter, Characterization and microanalysis of interfacial reactions in metal–matrix composite systems, J. Microsc. 185 (1997) 217–224.
[15] J. Wadsworth, F.H. Froes, Developments in metallic materials for aerospace applications, JOM 41 (1989) 12–19.
[16] L.U. Ogbuji, Development of oxide scale microstructure on single-crystal SiC, J. Mater. Sci. 16 (1981) 2753–2759.
[17] P. Schuster, Formation of cristobalite from silicon carbide, Mater. Res. Bull. 4 (1969) 311.
[18] F.J. Gotor, J.M. Criado, J. Malek, N. Koga, Kinetic analysis of solid-state reactions: the universality of master plots for analyzing isothermal and nonisothermal experiments, J. Phys. Chem. A 104 (2000) 10777–10782.
[19] A. Khawam, D.R. Flanagan, Solid-state kinetic models: basics and mathematical fundamentals, J. Phys. Chem. B 110 (2006) 17315–17328.
[20] C.F. Gutierrez-Gonzalez, E. Fernandez-Garcia, A. Fernandez, R. Torrecillas, S. Lopez-Esteban, Processing, spark plasma sintering, and mechanical behavior of alumina/titanium composites, J. Mater. Sci. 49 (2014) 3823–3830.
[21] P. Kofstad, High-temperature oxidation of titanium, J. Less Common Met. 12 (1967) 449–464.
[22] A.M. Ginstling, V.I. Brounshtein, Concerning the Diffusion Kinetics of Reactions in Spherical Particles, J. Appl. ChcilL USSR 23 (1950) 1327–1338.
[23] P. Kofstad, P.B. Anderson, O.J. Krudtaa, Oxidation of titanium in the temperature range 800–1200 °C, J. Less Common Met. 3 (1961) 89–97.
[24] J. Šesták, Rationale and fallacy of thermoanalytical kinetic patterns, J. Therm. Anal. Calorim. 110 (2011) 5–16.
[25] N. Cuadrado, J. Seuba, D. Casellas, M. Anglada, E. Jiménez-Piqué, Geometry of nanoindentation cube-corner cracks observed by FIB tomography: implication for fracture resistance estimation, J. Eur. Ceram. Soc. 35 (2015) 2949–2955.
[26] B.R. Lawn, E.R. Fuller, Equilibrium penny-like cracks in indentation fracture, J. Mater. Sci. 10 (1975) 2016–2024.
[27] Z. Chen, Y. Liu, H. Jiang, M. Liu, C.H. Wang, G.H. Cao, Microstructures and mechanical properties of Mn modified, Ti-Nb-based alloys, J. Alloy. Compd. 723 (2017) 1091–1097.
[28] P. Auerkari, Mechanical and physical properties of engineering alumina ceramics, Tech. Res. Cent. Finl. VTT Manuf. Technol. (1996) 3–36.
[29] S.A. Ponnusami, S. Turteltaub, S. van der Zwaag, Cohesive-zone modelling of crack nucleation and propagation in particulate composites, Eng. Fract. Mech. 149 (2015) 170–190.
[30] L. Boatemaa, M. Bosch, A.-S. Farle, G.-P. Bei, S. van der Zwaag, W.G. Sloof, Autonomous high temperature healing of surface cracks in Al_2O_3 containing Ti_2AlC particles, J. Am. Ceram. Soc. (2018) (Submitted for publication).